# Highlights

- Neural trajectories in the hippocampus exhibited greater variability during a working memory (WM) task compared to those in the entorhinal cortex and amygdala regions.

- The distance of neural trajectories between encoding and retrieval states in the hippocampus was memory-load dependent during a WM task.

- Hippocampal neural trajectories fluctuated between the encoding and retrieval states in a task-dependent manner during both baseline and sharp-wave ripple (SWR) periods.

- Hippocampal neural trajectories shifted from encoding to retrieval states during SWR period.

# Hippocampal neural fluctuations between memory encoding and retrieval states during a working memory task in humans

Yusuke Watanabe[a,*], Yuji Ikegaya[b,c,d], Takufumi Yanagisawa[a,e]

[a] *Institute for Advanced Cocreation studies, Osaka University, 2-2 Yamadaoka, Suita, 565-0871, Osaka, Japan*
[b] *Graduate School of Pharmaceutical Sciences, The University of Tokyo, 7-3-1 Hongo, Tokyo, 113-0033, Japan*
[c] *Institute for AI and Beyond, The University of Tokyo, 7-3-1 Hongo, Tokyo, 113-0033, Japan*
[d] *Center for Information and Neural Networks, National Institute of Information and Communications Technology, 1-4 Yamadaoka, Suita City, 565-0871, Osaka, Japan*
[e] *Department of Neurosurgery, Osaka University Graduate School of Medicine, 2-2 Yamadaoka, Osaka, 565-0871, Japan*

## Abstract

Working memory (WM) ~~underpins numerous~~ plays a vital role in many cognitive functions, ~~but its neural mechanisms remain partially described. Despite recognition~~ though the complex neural mechanisms that support its operation are not yet fully understood. Although the importance of the hippocampus and sharp-wave ripple complexes (SWRs) ~~— rapid, coordinated neural events in the hippocampus — for their roles~~ – fast, concurrent neural activities within the hippocampus – are acknowledged in memory consolidation and retrieval, their ~~contribution to~~ participation in WM tasks remains ~~ambiguous. The current study posits that the multivariate activity patterns in the hippocampus work in conjunction~~ somewhat ambiguous. Our study hypothesizes that multiunit activity patterns within the hippocampus cooperate synergistically with SWRs, ~~exhibiting unique~~ showcasing distinctive dynamism during WM tasks. ~~We conducted an extensive examination~~ To investigate this, we carried out a thorough analysis of a dataset ~~derived~~ sourced from intracranial electroencephalogram recordings taken from the medial temporal lobe (MTL) of nine ~~individuals with epilepsy during~~ epilepsy patients performing an eight-second Sternberg task. ~~The dataset was analyzed using~~ Employing Gaussian-process factor analysis~~to detect~~, we distinguished low-dimensional neural representations, or 'trajectories,' ~~in~~ within the MTL regions during the WM task. ~~Findings showed the greatest variation in the neural trajectory~~ Our findings showed that neural trajectories exhibited greater variation in the hippocampus compared to the entorhinal cortex and amygdala. ~~Furthermore, trajectory differences identified~~ Additionally, differences found in the trajectories between encoding and retrieval phases ~~were dependent~~ depended on memory load. ~~Critically~~Notably, hippocampal trajectories oscillated during the retrieval phase, ~~presenting task-related transitions~~ demonstrating task-dependent shifts between encoding and retrieval states, ~~including~~ along with baseline and SWR ~~episodes~~events. These oscillations transitioned from encoding to retrieval states in ~~tandem~~ sync with SWRs. ~~Our~~ Consequently, our findings underscore the ~~essential role~~ critical function of the hippocampus in ~~conducting WM tasks~~performing WM tasks, and suggest a compelling hypothesis for ~~future research: the functional~~ further investigation: the operational state of the hippocampus ~~transitions~~ shifts from encoding to retrieval during SWRs.

*Keywords:* working memory, WM, memory load, hippocampus, sharp-wave ripples, SWR, humans

Working memory (WM) ~~plays a crucial role in everyday life, and its neural underpinnings remain an area of ongoing research~~ is vitally important in daily activities and continues to be an active research area, specifically its neural basis. The hippocampus, ~~notably integral to memory, continues to be a primary focus of this investigation~~ known to be essential for memory, consistently remains at the center of this inquiry [1] [2] [3] [4] [5] [6] [7] [8] [9]. ~~Gaining insights into the role of the hippocampus~~Insights into the hippocampus's role in working memory ~~is vital to deepening~~ are

*Corresponding author. Tel: +81-6-6879-3652

crucial for advancing our understanding of cognitive processes ~~, hence fostering the progression of~~ and thereby promoting developments in cognitive training and interventions.

~~Current evidence suggests a transient~~Existing evidence proposes that a temporary, synchronized oscillation, ~~referred to~~ known as sharp-wave ripple (SWR) [10], is ~~linked~~ associated with several cognitive functions, such as memory replay [11] [12] [13] [14] [15], memory consolidation [16] [17] [18] [19], memory recall [20] [21] [22], ~~and~~ along with neural plasticity [23] [24]. ~~This evidence indicates the likelihood that SWR could be a critical component~~ These indications suggest that SWR might be an essential part of hippocampal processing, thus contributing to working memory performance. ~~However, research investigating the effects~~ Yet, studies examining the effect of SWRs on working memory ~~remains sparse [25], and is largely limited to rodent models participating~~ are limited [25] , with most research predominantly focusing on rodent models engaged in navigation tasks where the timing of memory acquisition and recall is not explicitly ~~distinguished~~outlined.

Recent studies ~~indicate~~ have illustrated that hippocampal neurons ~~exhibit~~ demonstrate low-dimensional representations during WM tasks. ~~Notably~~Specifically, the firing patterns of place cells [26] [27] [28] [29] [30], located in the hippocampus, ~~are observed to be encompassed~~ have been shown to exist within a dynamic, nonlinear three-dimensional hyperbolic geometry in rodents [31]. ~~Moreover, grid~~ Grid cells in the entorhinal cortex (EC)—the ~~dominant~~ primary pathway to the hippocampus [32] [33] [34]—~~displayed~~ showed a toroidal topology during exploration [35]. ~~Unfortunately~~However, these investigations ~~are~~ have been confined to spatial navigation tasks in rodents, thus ~~imposing limitations on~~ constraining the temporal resolution of WM tasks. The ~~applicability~~ implication of these findings ~~to~~ for human subjects and their ~~generalization~~ extrapolation beyond navigation tasks ~~remains to be established~~is yet to be confirmed.

~~Given these considerations, the current study aims to validate~~ Considering these factors, this study seeks to support the hypothesis that hippocampal neurons ~~exhibit distinctive representations in~~ represent low-dimensional spaces ~~, designated~~ distinctively, referenced here as 'neural trajectory,' ~~during WM tasks, most prominently within SWR periods . To evaluate this claim, we employed~~ particularly during SWR periods in WM tasks. To assess this proposition, we utilized a dataset of patients ~~performing~~ executing an eight-second Sternberg task ~~with~~ featuring high temporal resolution (1 s for fixation, 2 s for encoding, 3 s for ~~maintenance~~upkeep, and 2 s for retrieval) ~~,~~ while their intracranial electroencephalography signals (iEEG) within the medial temporal lobe (MTL) were being ~~monitored~~ recorded [36]. To ~~investigate~~ explore low-dimensional neural trajectories, we employed Gaussian-process factor analysis (GPFA), ~~a method renowned~~ an acclaimed strategy for analyzing neural population dynamics [37].

## 1. Methods

### 1.1. Dataset

A publicly available dataset [36] was used~~, which~~ . This dataset consists of nine epilepsy patients performing a modified Sternberg task~~. This task involves~~ , a task incorporating four phases: fixation (1s), encoding (2s), maintenance (3s), and retrieval (2s) [36]. ~~During~~ Throughout the encoding phase, participants were ~~exposed~~ introduced to four, six, or eight alphabet letters, ~~referred to~~ known as the set size. ~~Subsequently, they had to decide~~ These participants were then tasked to ascertain whether a probe letter, presented during the retrieval phase was previously ~~displayed~~ shown (the correct choice for the Match IN task) or not (the correct choice for the Mismatch OUT task). iEEG signals were recorded at a sampling rate of 32 kHz, within a frequency range of 0.5–5,000 Hz, using depth electrodes implanted in ~~the~~ various medial temporal lobe (MTL) regions~~:~~; these include the anterior head of the left and ~~the~~ right hippocampus (AHL and AHR), the posterior body of the hippocampus (PHL and PHR), the entorhinal cortex (ECL and ECR), and the amygdala (AL and AR), as ~~illustrated~~ depicted in Figure 1A and Table 1. ~~The~~ Subsequently, these iEEG signals were ~~subsequently~~ downsampled to a rate of 2 kHz. Correlations among variables, such as set size and correct rate, were investigated (Figure **??**S1). The timings of multiunit spikes were determined ~~by~~ using a spike sorting algorithm [38] ~~using~~ via the Combinato package (`https://github.com/jniediek/combinato`) (Figure 1C).

### 1.2. Calculation of neural trajectories using GPFA

Neural trajectories, ~~also termed~~ a.k.a. 'factors' (Figure 1D), in areas including the hippocampus, EC, and amygdala (Figure 1D), were ~~computed~~ calculated using GPFA [37] applied to the multiunit activity data for each session. GPFA was ~~performed~~ executed with the elephant package (`https://elephant.readthedocs.io/en/latest/reference/gpfa.html`). The bin size was set to 50 ms, with no overlaps. Each factor was z-normalized across all sessions. The Euclidean distance from the origin ($O$) was ~~then~~ subsequently calculated (Figure 1E).

For each trajectory within a region, ~~for instance~~e.g., AHL, *geometric medians* (~~i.e.,~~ $g_F$ for fixation, $g_E$ for encoding, $g_M$ for maintenance, and $g_R$ for retrieval phase) were ~~determined~~ ascertained by calculating the median coordinates of the trajectory during the four phases (Figure 1D). An optimal dimensionality for GPFA was identified as three using the elbow method, ~~which was~~ derived by investigating the log-likelihood values through a three-fold cross-validation approach (Figure 2B).

### 1.3. Identifying SWR candidates from hippocampal regions

Potential SWR events within the hippocampus were detected using a widely ~~accepted~~ adopted method [39]. LFP signals from a specific region of interest (ROI), such as AHL, were re-referenced by subtracting an averaged signal from locations outside the ROI (*e.g.*, AHR, PHL, PHR, ECL, ECR, AL, and AR) (see Figure 1A). The re-referenced LFP signals ~~were then filtered~~ then underwent filtering with a ripple-band filter (80–140 Hz) to identify ~~SWR candidates (=~~possible SWR candidates, dubbed SWR$^+$ candidates ~~)~~ (see Figure 1B). SWR detection ~~was conducted using~~ utilized a published tool (`https://github.com/Eden-Kramer-Lab/ripple_detection`) [40], with the bandpass range adjusted to 80–140 Hz for humans [21] [22], ~~different~~ deviating from the original 150–250 Hz range typically applied to rodents.

Control events for SWR$^+$ candidates, labeled as SWR$^-$ candidates, were identified by randomly shuffling the timestamps of SWR$^+$ candidates across all trials and subjects. The resulting SWR$^+$/SWR$^-$ candidates were then subjected to visual inspection ~~, as shown in~~ (Figure 1).

### 1.4. Defining SWRs from putative hippocampal CA1 regions

SWRs were distinguished from SWR candidates in presumptive CA1 regions. ~~Initially, these regions were defined as follows~~The regions were initially defined in the following manner: SWR$^+$/SWR$^-$ candidates in the hippocampus were projected into a two-dimensional space based on overlapping spike counts per unit ~~employing~~ using a supervised method ~~using~~ called UMAP (Uniform Manifold Approximation and Projection) [41] (Figure 4A). Clustering validation was performed by computing the silhouette score [42] from clustered samples (Table 2). Regions in the hippocampus, which scored above 0.6 on average across sessions (75th percentile) (Figure 4B), were ~~characterized as~~ considered to be presumed CA1 regions, thereby identifying five electrode positions ~~from~~ among five patients (Table 3).

SWR$^+$/SWR$^-$ candidates in ~~the~~ these assumed CA1 regions were ~~classified~~ reclassified as SWR$^+$/SWR$^-$, ~~thus relinquishing~~ hence losing their candidate status. The duration and ripple band peak amplitude of SWRs were observed to ~~follow~~ conform to log-normal distributions (Figure 44C & E). Each time period of SWR was partitioned ~~relative~~ in relation to the time from the SWR center into pre- (at −800 to −300 ms from SWR center), mid- (at −250 to +250 ms), and post-SWR (at +300 to +800 ms) times.

### 1.5. Statistical evaluation

~~The Brunner–Munzel test and the Kruskal-Wallis test~~ Statistical analyses were performed using the Brunner–Munzel and Kruskal-Wallis tests courtesy of the SciPy package in Python [43]. ~~Correlational analysis was performed by determining~~ The correlational analysis determined the rank of the observed correlation coefficient in its associated set-size-shuffled surrogate ~~using~~ via a custom Python script. The bootstrap test, on the other hand, was implemented using an in-house Python script.

## 2. Results

### 2.1. iEEG recording and neural trajectory in MTL regions during a Sternberg task

We leveraged a publicly available dataset for this analysis [36]. This dataset encompasses LFP signals

(Figure 1A) from MTL regions (Table 1) during a modified Sternberg task execution. We identified $SWR^+$ candidates from LFP signals filtered through the 80–140 Hz ripple band (Figure 1B), originating across all hippocampal regions (refer to Methods). Correspondingly, $SWR^-$ candidates were defined at identical timestamps) but shuffled across different trials (Figure 1). The dataset included multiunit spikes (Figure 1C) identified via a spike sorting algorithm [38]. By employing GPFA [37], and using the 50-ms binned multiunit activity with no overlaps, we determined the neural trajectories (or factors) of MTL regions by session and region (Figure 1D). We normalized each factor by session and region for instance, session #2 in AHL of subject #1. Subsequently, we calculated the Euclidean distance from the origin ($O$) (Figure 1E).

### 2.2. *Hippocampal neural trajectory correlation with a Sternberg task*

Figure 2A illustrates the cloud of median neural trajectories of 50 trials within the three main factor spaces. We determined the optimal embedding dimension for the GPFA model to be three, using the elbow method (Figure 2B). The trajectory distance from the origin ($O$) (represented as $||g_F||$, $||g_E||$, $||g_M||$, and $||g_R||$) in the hippocampus exceeded corresponding distances in the EC and amygdala (Figures 2C and D).[1]

Similarly, we computed the distances between the geometric medians of four phases, namely $||g_F g_E||$, $||g_F g_M||$, $||g_F g_R||$, $||g_E g_M||$, $||g_E g_R||$, and $||g_M g_R||$. The results indicated that the hippocampus displayed larger distances between phases than both the EC and amygdala. [2]

### 2.3. *Memory load-dependent neural trajectory distance between encoding and retrieval states in the hippocampus*

In terms of memory load in the Stenberg task, we identified a negative correlation between the correct rate of trials and set size (the number of letters to encode) (Figure 3A).[3] Similarly, a positive correlation was observed between the response time and set size (Figure 3B).[4].

Furthermore, we found a positive correlation between set size and the trajectory distance between the encoding and retrieval phases ($\log_{10}||g_E g_R||$) (Figure 3C).[5]. However, distances between other combinations of phases did not display statistically significant correlations (Figures 3D and S2).

### 2.4. *Detection of hippocampal SWR from putative CA1 regions*

For precision improvement in recording sites and SWR detection, we estimated the electrode placements in the CA1 regions of the hippocampus using distinct multiunit spike patterns during the SWR events. $SWR^+$/$SWR^-$ candidates from every session and hippocampal region were embedded in a two-dimensional space using UMAP (Figure 4A).[6] We used the silhouette score as a metric for quality of clustering (Figure 4B and Table 2). Recording sites with an average silhouette score exceeding 0.6 across all sessions were identified as putative CA1 regions.[7] (Tables 2 and 3). We identified five putative CA1 regions, four of which were not labeled as seizure onset zones (Table 1).

Subsequently, $SWR^+$/$SWR^-$ candidates within these putative CA1 regions were labeled as $SWR^+$ and $SWR^-$, respectively[8] (Table 3). Both $SWR^+$ and $SWR^-$

[1] Hippocampus: Distance = 1.11 [1.01], median [IQR], $n$ = 195,681 timepoints; EC: Distance = 0.94 [1.10], median [IQR], $n$ = 133,761 timepoints; Amygdala: Distance = 0.78 [0.88], median [IQR], $n$ = 165,281 timepoints.

[2] Hippocampus: Distance = 0.60 [0.70], median [IQR], $n$ = 8,772 combinations; EC: Distance = 0.28 [0.52], median [IQR], $n$ = 5,017 combinations ($p < 0.01$; Brunner–Munzel test); Amygdala: Distance = 0.24 [0.42], median [IQR], $n$ = 7,466 combinations ($p < 0.01$; Brunner–Munzel test).

[3] Correct rate: set size four (0.99 ±0.11, mean ±SD; $n$ = 333 trials) vs. set size six (0.93 ±0.26; $n$ = 278 trials; $p < 0.001$, Brunner–Munzel test with Bonferroni correction) and set size eight (0.87 ±0.34; $n$ = 275 trials; $p < 0.05$; Brunner–Munzel test with Bonferroni correction). Overall, $p < 0.001$ for Kruskal–Wallis test; correlation coefficient = -0.20, $p < 0.001$.

[4] Response time: set size four (1.26 ±0.45 s; $n$ = 333 trials) vs. set size six (1.53 ±0.91 s; $n$ = 278 trials) and set size eight (1.66 ±0.80 s; $n$ = 275 trials). All comparisons $p < 0.001$, Brunner–Munzel test with Bonferroni correction; $p < 0.001$ for Kruskal–Wallis test; correlation coefficient = 0.22, $p < 0.001$

[5] Correlation between set size and $\log_{10}(||g_E g_R||)$: correlation coefficient = 0.05, $p < 0.001$. Specific values: $||g_E g_R||$ = 0.54 [0.70] for set size four, $n$ = 447; $||g_E g_R||$ = 0.58 [0.66] for set size six, $n$ = 381; $||g_E g_R||$ = 0.61 [0.63] for set size eight, $n$ = 395.

[6] Consider the AHL in session #1 of subject #1, for illustration purposes.

[7] The identified regions were: AHL of subject #1, AHR of subject #3, PHL of subject #4, AHL of subject #6, and AHR of subject #9.

[8] These definitions led to equal counts for both categories: $SWR^+$ ($n$ = 1,170) and $SWR^-$ ($n$ = 1,170).

exhibited the same duration[9] (Figure 4C) due to their definitions, and followed a log-distribution. We observed an augmentation in $\text{SWR}^+$ incidence during the initial 400 ms of the retrieval phase[10] (Figure 4D). The peak ripple band amplitude of $\text{SWR}^+$ outpaced $\text{SWR}^-$ and followed a log-normal distribution (Figure 4E).[11].

### 2.5. *Transient changes in hippocampal neural trajectory during SWR*

We computed the distance of the trajectory from the origin ($O$) during SWR events in both the encoding and retrieval phases (Figure 5A). Observing the increase in distance during SWR as shown in Figure 5A, we differentiated each SWR into three stages: pre-, mid-, and post-SWR. Therefore, the distances from $O$ during those SWR periods are identified as $\|\text{pre-eSWR}^+\|$, $\|\text{mid-eSWR}^+\|$ among others.

$\|\text{mid-eSWR}^+\|$[12] was greater than $\|\text{pre-eSWR}^+\|$[13], and $\|\text{mid-rSWR}^+\|$[14] was larger than $\|\text{pre-rSWR}^+\|$ in both Match IN and Mismatch OUT tasks.[15].

### 2.6. *Visualization of hippocampal neural trajectory during SWR in two-dimensional spaces*

Following our observations of neural trajectory 'jumping' during SWR (Figure 5), we visualized the three-dimensional trajectories of pre-, mid-, and post-SWR events during the encoding and retrieval phases (Figure 6), the distance between which was found to be memory-load dependent (Figure 3).

To provide two-dimensional visualization, we linearly aligned peri-SWR trajectories by assigning $g_E$ at the origin (0, 0) and $g_R$ at ($\|g_E g_R\|$, 0). Post this, we rotated these aligned trajectories around the $g_E g_R$ axis (the x-axis). Thus, the distances from the origin in the original three-dimensional spaces are preserved in the two-dimensional equivalent.

The scatter plot within these two-dimensional spaces reveals characteristic distributions of peri-SWR trajectories based on phases and task types. For instance, one can observe that the magnitude of $\|\text{mid-eSWR}^+\|$ surpasses that of $\|\text{pre-eSWR}^+\|$ (Figure 6B), consistent with our earlier findings (Figure 5).

### 2.7. *Fluctuations of hippocampal neural trajectories between encoding and retrieval states*

Next, we examined trajectory *directions* in relation to $\overrightarrow{g_E g_R}$. The directions of SWRs were defined by the neural trajectory at −250 ms and +250 ms from their center, i.e., $\overrightarrow{\text{eSWR}^+}$.

We calculated the density of $\overrightarrow{\text{eSWR}} \cdot \overrightarrow{g_E g_R}$, $\overrightarrow{\text{rSWR}} \cdot \overrightarrow{g_E g_R}$, and $\overrightarrow{\text{eSWR}} \cdot \overrightarrow{\text{rSWR}}$ (Figures 7A–D). $\overrightarrow{\text{rSWR}^-} \cdot \overrightarrow{g_E g_R}$ displayed a biphasic distribution.

By taking the difference between the distribution of $\overrightarrow{\text{rSWR}^+} \cdot \overrightarrow{g_E g_R}$ (Figures 7A and B) and that of $\overrightarrow{\text{rSWR}^-} \cdot \overrightarrow{g_E g_R}$ (Figures 7C and D), we computed the contributions of SWR (Figures 7E and F), which revealed a shift in the direction of $\overrightarrow{g_E g_R}$ (Figures 7E and F: *red rectangles*).

Moreover, exclusively in the Mismatch OUT task, $\overrightarrow{\text{eSWR}^+} \cdot \overrightarrow{\text{rSWR}^+}$ was less than $\overrightarrow{\text{eSWR}^-} \cdot \overrightarrow{\text{rSWR}^-}$ (baseline periods) (Figure 7F: *pink circles*). In simpler terms, eSWR and rSWR pointed in the opposite direction only in the Mismatch OUT task but not in the Match IN task (Figure 7E: *pink circles*).

## 3. Discussion

## 4. Discussion

This study ~~hypothesized~~ proposed that within low-dimensional spaces during a working memory (WM) task in humans, hippocampal neurons ~~form~~ shape unique trajectories, ~~particularly~~ especially during sharp-wave ripple (SWR) periods. Initially, we projected the multiunit spikes ~~in~~ from medial temporal lobe (MTL) regions ~~were projected~~ onto three-dimensional spaces during a Sternberg task using Gaussian Process Factor Analysis (GPFA) (Figure 1D–E and Figure 2A). ~~The distance of the trajectory~~ We noted that the trajectory distance across WM phases ($\|g_F g_E\|$, $\|g_F g_M\|$, $\|g_F g_R\|$, $\|g_E g_M\|$, $\|g_E g_R\|$, and $\|g_M g_R\|$) was ~~notably~~

[9] These definitions led to equal durations for both categories: $\text{SWR}^+$ (93.0 [65.4] ms) and $\text{SWR}^-$ (93.0 [65.4] ms).

[10] $\text{SWR}^+$ increased against the bootstrap sample; 95th percentile = 0.42 [Hz]; $p < 0.05$.

[11] $\text{SWR}^+$ (3.05 [0.85] SD of baseline, median [IQR]; $n$ = 1,170) vs. $\text{SWR}^-$ (2.37 [0.33] SD of baseline, median [IQR]; $n$ = 1,170; $p <$ 0.001; Brunner–Munzel test).

[12] 1.25 [1.30], median [IQR], $n$ = 1,281, in Match IN task; 1.12 [1.35], median [IQR], $n$ = 1,163, in Mismatch OUT task

[13] 1.08 [1.07], median [IQR], $n$ = 1,149, in Match IN task; 0.90 [1.12], median [IQR], $n$ = 1,088, in Mismatch OUT task

[14] 1.32 [1.24], median [IQR], $n$ = 935, in Match IN task; 1.15 [1.26], median [IQR], $n$ = 891, in Mismatch OUT task

[15] 1.19 [0.96], median [IQR], $n$ = 673, in Match IN task; 0.94 [0.88], median [IQR], $n$ = 664, in Mismatch OUT task

significantly larger in the hippocampus than in the ~~EC~~ entorhinal cortex (EC) and amygdala (Figure 2E)~~, indicating~~ . This revelation indicated dynamic neural activity in the hippocampus during the WM task. ~~Further, in the hippocampus,~~ Furthermore, a positive correlation between the trajectory distance ~~between the encoding and retrieval phases~~ from the encoding to the retrieval phase ($\|g_F g_E\|$) ~~exhibited a positive correlation with memory load~~ and memory load was seen in the hippocampus (Figure 3C–D), ~~reflecting~~ which reflected WM processing. ~~The~~ Transient increases were discovered in the hippocampal neural trajectory ~~was found to increase transiently~~ during SWRs (Figure 5). ~~Finally~~Lastly, the hippocampal neural trajectory switched between encoding and retrieval states, ~~moving~~ transitioning from encoding to retrieval during SWR events (Figure 7). These findings not only ~~explain various facets~~ elucidate varying aspects of hippocampal neural activity during a WM task in humans but also offer new insights into how SWRs influence the switch in neural states.

~~We found that the~~ The distance of the neural trajectory across the phases was discovered to be greater in the hippocampus compared to that in the EC and amygdala, even when considering the distance from $O$ in these regions (Figure 2C–E). This ~~supports~~ evidence backs the involvement of the hippocampus in the WM task, ~~aligning with previous reports of hippocampal persistent firing~~ in agreement with prior reports of persistent firing within the hippocampus during the maintenance phase [3] [4] [5] [6]. However, when ~~we applied GPFA~~ GPFA was applied to multiunit activity ~~during a 1-second level resolution of~~ at 1-second-level resolution during the WM task, ~~we observed that~~ the neural trajectory in low-dimensional space ~~showed a memory-load dependency~~ displayed a memory load dependence between the encoding and retrieval phases, ~~symbolized~~ expressed as $\|g_E g_R\|$ (Figure 3). ~~These findings corroborate the association of the hippocampus with~~ This result reinforces the association between the hippocampus and WM processing.

~~Our analysis was confined to~~ The analysis concentrated on putative CA1 regions (Figure 4), ~~which was bolstered by several~~ corroborated by multiple factors. This specific focus ~~stems~~ originates from established observations that SWRs synchronize with spike bursts of interneurons and pyramidal neurons [44] [45] [46] [47], potentially within a 50 $\mu$m radius of the recording site [48]. We ~~further identified an increased~~ also noticed a heightened incidence of SWRs during the first 0–400 ms of the retrieval phase (Figure 4D)~~. This finding harmonizes with previous reports of heightened~~ , which is consistent with previous findings of increased SWR occurrence preceding spontaneous verbal recall [21] [22], ~~supporting~~ reinforcing our results under a triggered retrieval condition. The observed log-normal distributions of both SWR duration and ripple band peak amplitude in this ~~study~~ research (Figure 4C & E) ~~is in accordance with~~ conform to the consensus in this field [39]. ~~As a result, our decision to restrict~~ Consequently, limiting recording sites to putative CA1 regions likely ~~contributed to enhancing~~ improved the accuracy of SWR detection. However, the increase in trajectory distance from $O$ during SWRs (Figure 5) ~~might have been skewed~~ may have been biased towards higher values due to channel selection. ~~However~~Nevertheless, this potential bias does not ~~substantially challenge our primary~~ significantly challenge our main findings.

Interestingly, ~~during the retrieval phase, the~~ trajectory directions oscillated between encoding and retrieval states during both baseline and SWR periods in the retrieval phase (Figure 7C & D). Moreover, the balance of this oscillation ~~shifted from encoding to~~ switched from the encoding state to the retrieval state during SWR events (Figure 7 E & F). These results ~~are consistent~~ align with previous reports on the role of SWR in memory retrieval [21] [22]. Our findings ~~highlight a new understanding~~shed a new light, suggesting that SWRs occur when the hippocampal representation transitions from encoding to retrieval states. ~~Therefore, these results reveal~~ Thus, these findings unmask two novel aspects of hippocampal representations~~, including~~ : (i) neuronal oscillation between encoding and retrieval states during a WM task and (ii) SWR ~~serving~~ acting as a trigger for ~~changing~~ shifting neural states.

~~Furthermore~~Additionally, our study ~~uncovered~~ unveiled WM-task type-specific differences between encoding- and retrieval-SWRs (Figure 7E–F). ~~Notably~~Importantly, opposing movements of encoding-SWR (eSWR) and retrieval-SWR (rSWR) were not ~~observed~~ demonstrated in the Match IN task but were ~~apparent~~ clear in the Mismatch OUT task. These

~~observations~~ results can be explained by ~~the~~ memory engram theory [49]~~. Particularly,~~ , which posits that the Match In task provided participants with previously presented letters, ~~contrastingly,~~ whereas the Mismatch OUT task introduced a new letter not present in the encoding phase. These interpretations ~~underscore~~ underline the significant role of SWR in human cognitive processes.

In conclusion, ~~the present~~ this investigation demonstrated that hippocampal activity oscillates between encoding and retrieval states during a WM task and uniquely transitions from encoding to retrieval during SWR ~~incidents~~events. These findings ~~provide meaningful~~ offer substantial insight into the neural ~~counterparts~~ mechanisms and functionality of working memory in the hippocampus.

## References


[1] W. B. Scoville, B. Milner, LOSS OF RECENT MEMORY AFTER BILATERAL HIPPOCAMPAL LESIONS, Journal of Neurology, Neurosurgery, and Psychiatry 20 (1) (1957) 11–21.
URL https://www.ncbi.nlm.nih.gov/pmc/articles/PMC497229/

[2] L. R. Squire, The Legacy of Patient H.M. for Neuroscience, Neuron 61 (1) (2009) 6–9. doi:10.1016/j.neuron.2008.12.023.
URL https://www.ncbi.nlm.nih.gov/pmc/articles/PMC2649674/

[3] E. Boran, T. Fedele, P. Klaver, P. Hilfiker, L. Stieglitz, T. Grunwald, J. Sarnthein, Persistent hippocampal neural firing and hippocampal-cortical coupling predict verbal working memory load, Science Advances 5 (3) (2019) eaav3687. doi:10.1126/sciadv.aav3687.
URL https://www.science.org/doi/10.1126/sciadv.aav3687

[4] J. Kamiński, S. Sullivan, J. M. Chung, I. B. Ross, A. N. Mamelak, U. Rutishauser, Persistently active neurons in human medial frontal and medial temporal lobe support working memory, Nature Neuroscience 20 (4) (2017) 590–601, number: 4 Publisher: Nature Publishing Group. doi:10.1038/nn.4509.
URL https://www.nature.com/articles/nn.4509

[5] S. Kornblith, R. Q. Quiroga, C. Koch, I. Fried, F. Mormann, Persistent Single-Neuron Activity during Working Memory in the Human Medial Temporal Lobe, Current Biology 27 (7) (2017) 1026–1032, publisher: Elsevier. doi:10.1016/j.cub.2017.02.013.
URL https://www.cell.com/current-biology/abstract/S0960-9822(17)30149-5

[6] M. C. M. Faraut, A. A. Carlson, S. Sullivan, O. Tudusciuc, I. Ross, C. M. Reed, J. M. Chung, A. N. Mamelak, U. Rutishauser, Dataset of human medial temporal lobe single neuron activity during declarative memory encoding and recognition, Scientific Data 5 (1) (2018) 180010, number: 1 Publisher: Nature Publishing Group. doi:10.1038/sdata.2018.10.
URL https://www.nature.com/articles/sdata201810

[7] A. A. Borders, C. Ranganath, A. P. Yonelinas, The hippocampus supports high-precision binding in visual working memory, Hippocampus 32 (3) (2022) 217–230. doi:10.1002/hipo.23401.

[8] J. Li, D. Cao, S. Yu, X. Xiao, L. Imbach, L. Stieglitz, J. Sarnthein, T. Jiang, Functional specialization and interaction in the amygdala-hippocampus circuit during working memory processing, Nature Communications 14 (1) (2023) 2921, number: 1 Publisher: Nature Publishing Group. doi:10.1038/s41467-023-38571-w.
URL https://www.nature.com/articles/s41467-023-38571-w

[9] V. Dimakopoulos, P. Mégevand, L. H. Stieglitz, L. Imbach, J. Sarnthein, Information flows from hippocampus to auditory cortex during replay of verbal working memory items, eLife 11 (2022) e78677, publisher: eLife Sciences Publications, Ltd. doi:10.7554/eLife.78677.
URL https://doi.org/10.7554/eLife.78677

[10] G. Buzsáki, Hippocampal sharp wave-ripple: A cognitive biomarker for episodic memory and planning, Hippocampus 25 (10) (2015) 1073–1188, _eprint: https://onlinelibrary.wiley.com/doi/pdf/10.1002/hipo.22488. doi:https://doi.org/10.1002/hipo.22488.
URL https://onlinelibrary.wiley.com/doi/abs/10.1002/hipo.22488

[11] M. A. Wilson, B. L. McNaughton, Reactivation of hippocampal ensemble memories during sleep, Science (New York, N.Y.) 265 (5172) (1994) 676–679. doi:10.1126/science.8036517.

[12] Z. Nádasdy, H. Hirase, A. Czurkó, J. Csicsvari, G. Buzsáki, Replay and Time Compression of Recurring Spike Sequences in the Hippocampus, Journal of Neuroscience 19 (21) (1999) 9497–9507, publisher: Society for Neuroscience Section: ARTICLE. doi:10.1523/JNEUROSCI.19-21-09497.1999.
URL https://www.jneurosci.org/content/19/21/9497

[13] A. K. Lee, M. A. Wilson, Memory of sequential experience in the hippocampus during slow wave sleep, Neuron 36 (6) (2002) 1183–1194. doi:10.1016/s0896-6273(02)01096-6.

[14] K. Diba, G. Buzsáki, Forward and reverse hippocampal place-cell sequences during ripples, Nature Neuroscience 10 (10) (2007) 1241–1242, number: 10 Publisher: Nature Publishing Group. doi:10.1038/nn1961.
URL https://www.nature.com/articles/nn1961

[15] T. J. Davidson, F. Kloosterman, M. A. Wilson, Hippocampal replay of extended experience, Neuron 63 (4) (2009) 497–507. doi:10.1016/j.neuron.2009.07.027.

[16] G. Girardeau, K. Benchenane, S. I. Wiener, G. Buzsáki, M. B. Zugaro, Selective suppression of hippocampal ripples impairs spatial memory, Nature Neuroscience 12 (10) (2009) 1222–1223. doi:10.1038/nn.2384.
URL http://www.nature.com/articles/nn.2384

[17] V. Ego-Stengel, M. A. Wilson, Disruption of ripple-associated hippocampal activity during rest impairs spatial learning in the rat, Hippocampus 20 (1) (2010) 1–10. doi:10.1002/hipo.20707.

[18] A. Fernández-Ruiz, A. Oliva, E. Fermino de Oliveira,

F. Rocha-Almeida, D. Tingley, G. Buzsáki, Long-duration hippocampal sharp wave ripples improve memory, Science (New York, N.Y.) 364 (6445) (2019) 1082–1086. doi:10.1126/science.aax0758.
URL https://www.ncbi.nlm.nih.gov/pmc/articles/PMC6693581/

[19] J. Kim, A. Joshi, L. Frank, K. Ganguly, Cortical–hippocampal coupling during manifold exploration in motor cortex, Nature (2022) 1–8Publisher: Nature Publishing Group. doi:10.1038/s41586-022-05533-z.
URL https://www.nature.com/articles/s41586-022-05533-z

[20] C.-T. Wu, D. Haggerty, C. Kemere, D. Ji, Hippocampal awake replay in fear memory retrieval, Nature Neuroscience 20 (4) (2017) 571–580. doi:10.1038/nn.4507.

[21] Y. Norman, E. M. Yeagle, S. Khuvis, M. Harel, A. D. Mehta, R. Malach, Hippocampal sharp-wave ripples linked to visual episodic recollection in humans, Science 365 (6454) (2019) eaax1030. doi:10.1126/science.aax1030.
URL https://www.sciencemag.org/lookup/doi/10.1126/science.aax1030

[22] Y. Norman, O. Raccah, S. Liu, J. Parvizi, R. Malach, Hippocampal ripples and their coordinated dialogue with the default mode network during recent and remote recollection, Neuron 109 (17) (2021) 2767–2780.e5, publisher: Elsevier. doi:10.1016/j.neuron.2021.06.020.
URL https://www.cell.com/neuron/abstract/S0896-6273(21)00461-X

[23] C. J. Behrens, L. P. van den Boom, L. de Hoz, A. Friedman, U. Heinemann, Induction of sharp wave–ripple complexes in vitro and reorganization of hippocampal networks, Nature Neuroscience 8 (11) (2005) 1560–1567, number: 11 Publisher: Nature Publishing Group. doi:10.1038/nn1571.
URL https://www.nature.com/articles/nn1571

[24] H. Norimoto, K. Makino, M. Gao, Y. Shikano, K. Okamoto, T. Ishikawa, T. Sasaki, H. Hioki, S. Fujisawa, Y. Ikegaya, Hippocampal ripples down-regulate synapses, Science (New York, N.Y.) 359 (6383) (2018) 1524–1527. doi:10.1126/science.aao0702.

[25] S. P. Jadhav, C. Kemere, P. W. German, L. M. Frank, Awake Hippocampal Sharp-Wave Ripples Support Spatial Memory, Science 336 (6087) (2012) 1454–1458, publisher: American Association for the Advancement of Science. doi:10.1126/science.1217230.
URL https://www.science.org/doi/abs/10.1126/science.1217230

[26] J. O'Keefe, J. Dostrovsky, The hippocampus as a spatial map: Preliminary evidence from unit activity in the freely-moving rat, Brain Research 34 (1971) 171–175, place: Netherlands Publisher: Elsevier Science. doi:10.1016/0006-8993(71)90358-1.

[27] J. O'Keefe, Place units in the hippocampus of the freely moving rat, Experimental Neurology 51 (1) (1976) 78–109. doi:10.1016/0014-4886(76)90055-8.
URL https://www.sciencedirect.com/science/article/pii/0014488676900558

[28] A. D. Ekstrom, M. J. Kahana, J. B. Caplan, T. A. Fields, E. A. Isham, E. L. Newman, I. Fried, Cellular networks underlying human spatial navigation, Nature 425 (6954) (2003) 184–188, number: 6954 Publisher: Nature Publishing Group. doi:10.1038/nature01964.
URL https://www.nature.com/articles/nature01964

[29] K. B. Kjelstrup, T. Solstad, V. H. Brun, T. Hafting, S. Leutgeb, M. P. Witter, E. I. Moser, M.-B. Moser, Finite Scale of Spatial Representation in the Hippocampus, Science 321 (5885) (2008) 140–143, publisher: American Association for the Advancement of Science. doi:10.1126/science.1157086.
URL https://www.science.org/doi/abs/10.1126/science.1157086

[30] C. D. Harvey, F. Collman, D. A. Dombeck, D. W. Tank, Intracellular dynamics of hippocampal place cells during virtual navigation, Nature 461 (7266) (2009) 941–946, number: 7266 Publisher: Nature Publishing Group. doi:10.1038/nature08499.
URL https://www.nature.com/articles/nature08499

[31] H. Zhang, P. D. Rich, A. K. Lee, T. O. Sharpee, Hippocampal spatial representations exhibit a hyperbolic geometry that expands with experience, Nature Neuroscience (Dec. 2022). doi:10.1038/s41593-022-01212-4.
URL https://www.nature.com/articles/s41593-022-01212-4

[32] P. A. Naber, F. H. Lopes da Silva, M. P. Witter, Reciprocal connections between the entorhinal cortex and hippocampal fields CA1 and the subiculum are in register with the projections from CA1 to the subiculum, Hippocampus 11 (2) (2001) 99–104, _eprint: https://onlinelibrary.wiley.com/doi/pdf/10.1002/hipo.1028. doi:10.1002/hipo.1028.
URL https://onlinelibrary.wiley.com/doi/abs/10.1002/hipo.1028

[33] N. M. van Strien, N. L. M. Cappaert, M. P. Witter, The anatomy of memory: an interactive overview of the parahippocampal–hippocampal network, Nature Reviews Neuroscience 10 (4) (2009) 272–282, number: 4 Publisher: Nature Publishing Group. doi:10.1038/nrn2614.
URL https://www.nature.com/articles/nrn2614

[34] B. A. Strange, M. P. Witter, E. S. Lein, E. I. Moser, Functional organization of the hippocampal longitudinal axis, Nature Reviews Neuroscience 15 (10) (2014) 655–669, number: 10 Publisher: Nature Publishing Group. doi:10.1038/nrn3785.
URL https://www.nature.com/articles/nrn3785

[35] R. J. Gardner, E. Hermansen, M. Pachitariu, Y. Burak, N. A. Baas, B. A. Dunn, M.-B. Moser, E. I. Moser, Toroidal topology of population activity in grid cells, Nature 602 (7895) (2022) 123–128, number: 7895 Publisher: Nature Publishing Group. doi:10.1038/s41586-021-04268-7.
URL https://www.nature.com/articles/s41586-021-04268-7

[36] E. Boran, T. Fedele, A. Steiner, P. Hilfiker, L. Stieglitz, T. Grunwald, J. Sarnthein, Dataset of human medial temporal lobe neurons, scalp and intracranial EEG during a verbal working memory task, Scientific Data 7 (1) (2020) 30, number: 1 Publisher: Nature Publishing Group. doi:10.1038/s41597-020-0364-3.
URL https://www.nature.com/articles/s41597-020-0364-3

[37] B. M. Yu, J. P. Cunningham, G. Santhanam, S. I. Ryu, K. V. Shenoy, M. Sahani, Gaussian-Process Factor Analysis for

Low-Dimensional Single-Trial Analysis of Neural Population Activity, Journal of Neurophysiology 102 (1) (2009) 614–635. doi:10.1152/jn.90941.2008.
URL https://www.ncbi.nlm.nih.gov/pmc/articles/PMC2712272/

[38] J. Niediek, J. Boström, C. E. Elger, F. Mormann, Reliable Analysis of Single-Unit Recordings from the Human Brain under Noisy Conditions: Tracking Neurons over Hours, PLOS ONE 11 (12) (2016) e0166598, publisher: Public Library of Science. doi:10.1371/journal.pone.0166598.
URL https://journals.plos.org/plosone/article?id=10.1371/journal.pone.0166598

[39] A. A. Liu, S. Henin, S. Abbaspoor, A. Bragin, E. A. Buffalo, J. S. Farrell, D. J. Foster, L. M. Frank, T. Gedankien, J. Gotman, J. A. Guidera, K. L. Hoffman, J. Jacobs, M. J. Kahana, L. Li, Z. Liao, J. J. Lin, A. Losonczy, R. Malach, M. A. van der Meer, K. McClain, B. L. McNaughton, Y. Norman, A. Navas-Olive, L. M. de la Prida, J. W. Rueckemann, J. J. Sakon, I. Skelin, I. Soltesz, B. P. Staresina, S. A. Weiss, M. A. Wilson, K. A. Zaghloul, M. Zugaro, G. Buzsáki, A consensus statement on detection of hippocampal sharp wave ripples and differentiation from other fast oscillations, Nature Communications 13 (1) (2022) 6000, number: 1 Publisher: Nature Publishing Group. doi:10.1038/s41467-022-33536-x.
URL https://www.nature.com/articles/s41467-022-33536-x

[40] K. Kay, M. Sosa, J. E. Chung, M. P. Karlsson, M. C. Larkin, L. M. Frank, A hippocampal network for spatial coding during immobility and sleep, Nature 531 (7593) (2016) 185–190. doi:10.1038/nature17144.

[41] L. McInnes, J. Healy, N. Saul, L. Großberger, UMAP: Uniform Manifold Approximation and Projection, Journal of Open Source Software 3 (29) (2018) 861. doi:10.21105/joss.00861.
URL https://joss.theoj.org/papers/10.21105/joss.00861

[42] P. J. Rousseeuw, Silhouettes: A graphical aid to the interpretation and validation of cluster analysis, Journal of Computational and Applied Mathematics 20 (1987) 53–65. doi:10.1016/0377-0427(87)90125-7.
URL https://www.sciencedirect.com/science/article/pii/0377042787901257

[43] P. Virtanen, R. Gommers, T. E. Oliphant, M. Haberland, T. Reddy, D. Cournapeau, E. Burovski, P. Peterson, W. Weckesser, J. Bright, S. J. van der Walt, M. Brett, J. Wilson, K. J. Millman, N. Mayorov, A. R. J. Nelson, E. Jones, R. Kern, E. Larson, C. J. Carey, Polat, Y. Feng, E. W. Moore, J. VanderPlas, D. Laxalde, J. Perktold, R. Cimrman, I. Henriksen, E. A. Quintero, C. R. Harris, A. M. Archibald, A. H. Ribeiro, F. Pedregosa, P. van Mulbregt, SciPy 1. 0 Contributors, SciPy 1.0: fundamental algorithms for scientific computing in Python, Nature Methods 17 (2020) 261–272, aDS Bibcode: 2020NatMe..17..261V. doi:10.1038/s41592-019-0686-2.
URL https://ui.adsabs.harvard.edu/abs/2020NatMe..17..261V

[44] G. Buzsáki, Two-stage model of memory trace formation: a role for "noisy" brain states, Neuroscience 31 (3) (1989) 551–570. doi:10.1016/0306-4522(89)90423-5.

[45] M. L. V. Quyen, A. Bragin, R. Staba, B. Crépon, C. L. Wilson, J. Engel, Cell Type-Specific Firing during Ripple Oscillations in the Hippocampal Formation of Humans, Journal of Neuroscience 28 (24) (2008) 6104–6110, publisher: Society for Neuroscience Section: Brief Communications. doi:10.1523/JNEUROSCI.0437-08.2008.
URL https://www.jneurosci.org/content/28/24/6104

[46] S. Royer, B. V. Zemelman, A. Losonczy, J. Kim, F. Chance, J. C. Magee, G. Buzsáki, Control of timing, rate and bursts of hippocampal place cells by dendritic and somatic inhibition, Nature Neuroscience 15 (5) (2012) 769–775, number: 5 Publisher: Nature Publishing Group. doi:10.1038/nn.3077.
URL https://www.nature.com/articles/nn.3077

[47] N. Hájos, M. R. Karlócai, B. Németh, I. Ulbert, H. Monyer, G. Szabó, F. Erdélyi, T. F. Freund, A. I. Gulyás, Input-output features of anatomically identified CA3 neurons during hippocampal sharp wave/ripple oscillation in vitro, The Journal of Neuroscience: The Official Journal of the Society for Neuroscience 33 (28) (2013) 11677–11691. doi:10.1523/JNEUROSCI.5729-12.2013.

[48] E. W. Schomburg, C. A. Anastassiou, G. Buzsáki, C. Koch, The Spiking Component of Oscillatory Extracellular Potentials in the Rat Hippocampus, The Journal of Neuroscience 32 (34) (2012) 11798–11811. doi:10.1523/JNEUROSCI.0656-12.2012.
URL https://www.ncbi.nlm.nih.gov/pmc/articles/PMC3459239/

[49] X. Liu, S. Ramirez, P. T. Pang, C. B. Puryear, A. Govindarajan, K. Deisseroth, S. Tonegawa, Optogenetic stimulation of a hippocampal engram activates fear memory recall, Nature 484 (7394) (2012) 381–385, number: 7394 Publisher: Nature Publishing Group. doi:10.1038/nature11028.
URL https://www.nature.com/articles/nature11028

## Contributors

Y.W. and T.Y. conceptualized the study; Y.W. performed the data analysis; Y.W. and T.Y. wrote the original draft; and all authors reviewed the final manuscript.

## Acknowledgments

This research was funded by a grant from the Exploratory Research for Advanced Technology (JPMJER1801).

## Declaration of Interests

The authors declare that they have no competing interests.

### Data and code availability

The data is available on G-Node (`https://doi.gin.g-node.org/10.12751/g-node.d76994/`).
The source code is available on GitHub (`https://github.com/yanagisawa-lab/hippocampal-neural-fluctuation-during-a-WM-task-in-humans`).

### Inclusion and Diversity Statement

We support inclusive, diverse, and equitable conduct of research.

### Declaration of Generative AI in Scientific Writing

The authors employed ChatGPT, provided by OpenAI, for enhancing the manuscript's English language quality. After incorporating the suggested improvements, the authors meticulously revised the content. Ultimate responsibility for the final content of this publication rests entirely with the authors.

## Tables

| Subject ID | of sessions | AHL | AHR | PHL | PHR | ECL | ECR | AL | AR | SOZ |
|---|---|---|---|---|---|---|---|---|---|---|
| 1 | 4 | o | x | o | o | o | x | o | x | "AHR, LR" |
| 2 | 7 | o | o | o | o | o | o | o | o | "AHR, PHR" |
| 3 | 3 | o | o | o | o | o | o | o | x | "AHL, PHL" |
| 4 | 2 | o | o | o | o | o | o | o | o | "AHL, AHR, PHL, PHR" |
| 5 | 3 | o | x | x | o | x | x | o | x | DRR |
| 6 | 6 | o | o | o | o | o | o | o | o | "AHL, PHL, ECL, AL" |
| 7 | 4 | o | o | o | o | o | o | o | o | "AHR, PHR" |
| 8 | 5 | o | o | o | o | o | o | o | o | ECR |
| 9 | 2 | o | o | o | o | o | o | o | o | "ECR, AR" |

**Table 1 – Distribution of Electrodes within the Dataset**

This figure ~~represents~~ depicts the ~~electrode placements and~~ locations of the electrodes as well as the seizure onset zones. ~~Regions designated with~~ The regions marked by an "o" ~~were available~~ denote their inclusion in the dataset, ~~whereas~~ while those ~~marked with~~ identified by an "x" (~~*navy*~~*in navy*) ~~were not present~~are absent. ~~Abbreviations include~~The abbreviations used are: AHL, left hippocampal head; AHR, right hippocampal head; PHL, left hippocampal body; PHR, right hippocampal body; ECL, left entorhinal cortex; ECR, right entorhinal cortex; AL, left amygdala; AR, right amygdala; and SOZ~~symbolizes the~~, which stands for seizure onset zone.

| Subject | AHL | AHR | PHL | PHR |
|---|---|---|---|---|
| 1 | 0.60 ± 0.14 | n.a. | n.a. | 0.1 ± 0 |
| 2 | 0.21 ± 0.16 | 0.17 ± 0.21 | 0.18 ± 0.22 | 0.20 ± 0.15 |
| 3 | 0.40 ± 0.42 | 0.83 ± 0.12 | n.a. | n.a. |
| 4 | 0.10 ± 0.00 | 0.10 ± 0.00 | 0.90 ± 0.00 | 0.10 ± 0.14 |
| 5 | n.a. | n.a. | n.a. | n.a. |
| 6 | 0.63 ± 0.06 | n.a. | n.a. | 0.27 ± 0.06 |
| 7 | 0.10 ± 0.00 | 0.35 ± 0.35 | 0.37 ± 0.47 | 0.10 ± 0.00 |
| 8 | 0.13 ± 0.10 | n.a. | 0.28 ± 0.49 | n.a. |
| 9 | n.a. | 0.85 ± 0.07 | 0.15 ± 0.07 | n.a. |

**Table 2 – Silhouette score of UMAP clustering for $SWR^+$ candidates and $SWR^-$ candidates**

The silhouette scores (mean ± SD across sessions per subject) for UMAP clustering of SWR+ candidates and SWR candidates ~~(Figure 4A)~~ were ~~calculated based on their~~ computed from the corresponding multiunit spike patterns~~(~~. The mean values were 0.205, with a standard deviation of 0.285, and median [IQR]; (Figure 4A and 4B).

| Subject ID | of sessions | of trials | ROI | of SWRs | SWR incidence [Hz] |
|---|---|---|---|---|---|
| 1 | 2 | 100 | AHL | 274 | 0.34 |
| 3 | 2 | 97 | AHR | 325 | 0.42 |
| 4 | 2 | 99 | PHL | 202 | 0.26 |
| 6 | 2 | 100 | AHL | 297 | 0.37 |
| 9 | 2 | 97 | AHR | 72 | 0.09 |
| Total = 10 | Total = 493 | "Total = 1,170" | 0.30 ± 0.13 (mean ± SD) | | |

**Table 3** – ~~**Accounting for Defined SWR Events**~~ **Accounting for Specified SWR Events**

The table ~~collates~~ collects statistics ~~of~~ pertaining to the putative CA1 regions and SWR events. ~~Only~~ To minimize sampling bias, only the first two sessions (sessions 1 and 2) from each subject were ~~considered to minimize sampling bias~~taken into consideration.

**Figures**

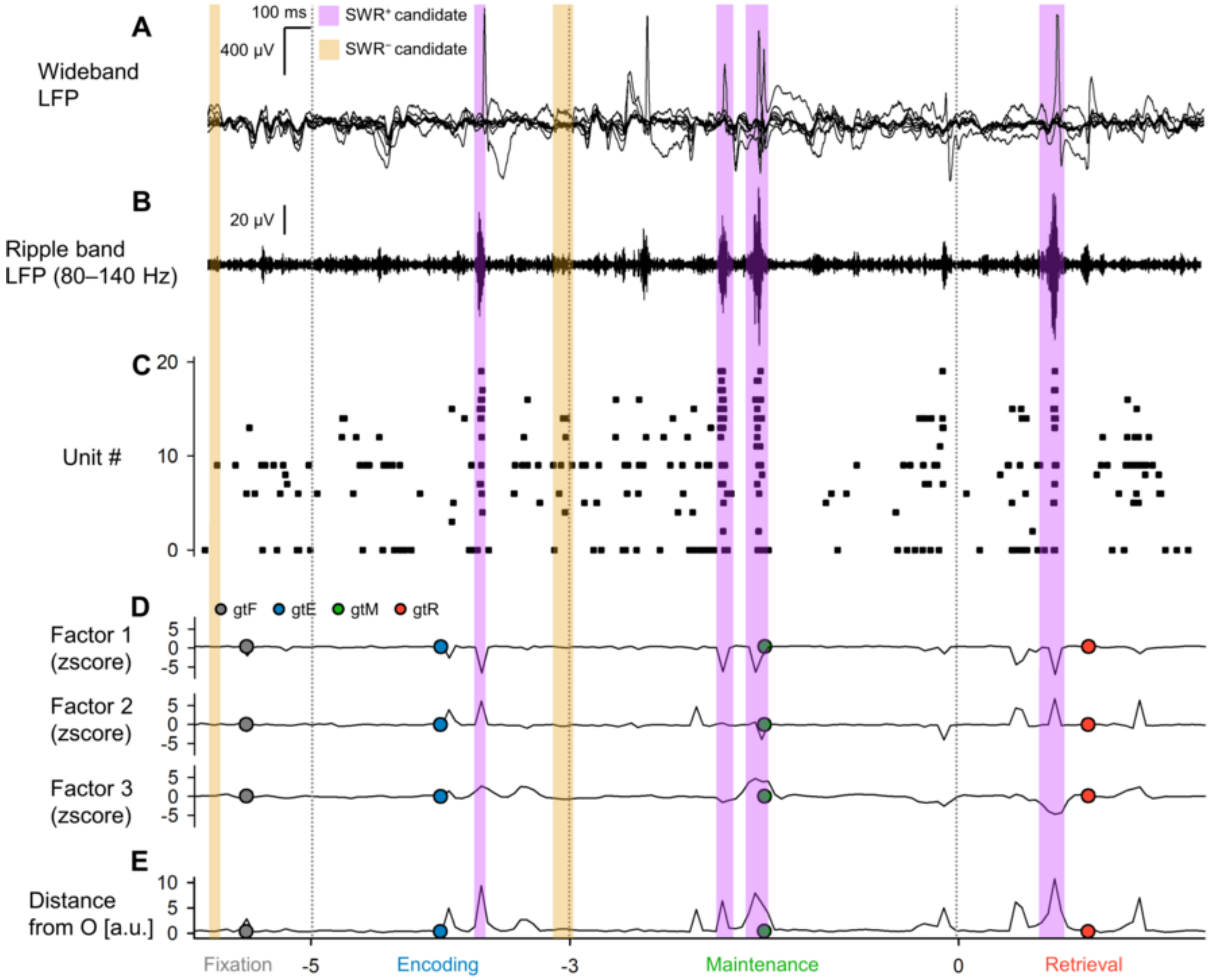


**Figure 1 – Local Field Potentials (LFP), Multiunit Activity, and Neural Trajectories in the Hippocampus During a Modified Sternberg Task**

***A.*** ~~These~~ The presented traces ~~show~~ illustrate representative wideband LFP intracranial EEG (iEEG) signals, recorded from the left hippocampal head ~~. The~~ while the subject ~~performed~~ was performing a modified Sternberg working memory task~~,~~ ~~which includes~~. This included phases of fixation (1 s, *gray*), encoding (2 s, *blue*), maintenance (3 s, *green*), and retrieval (2 s, *red*). ***B.*** ~~We then present~~ Subsequently, the corresponding ripple band LFP traces are delineated. ***C.*** The raster plot ~~depicts~~ represents multiunit spikes ~~taken~~ drawn from the LFP traces, sorted ~~using~~ by a ~~spike~~ reliable spike-sorting algorithm [38]. ***D.*** ~~Subsequently~~Following that, we ~~illustrate~~ portray the neural trajectories, which ~~are calculated by~~ have been computed using GPFA on spike counts per unit ~~with~~ within 50-ms bins. Each phase's geometric median is ~~marked~~ denoted by ~~the~~ dot circles. ***E.*** The ~~trajectory's~~ distance of the trajectory from the origin *O* is ~~portrayed~~presented, with *purple* and *yellow* rectangles indicating the timings for SWR$^+$ candidates and SWR$^-$ candidates (~~considered~~ acting as controls for SWR$^+$), respectively.

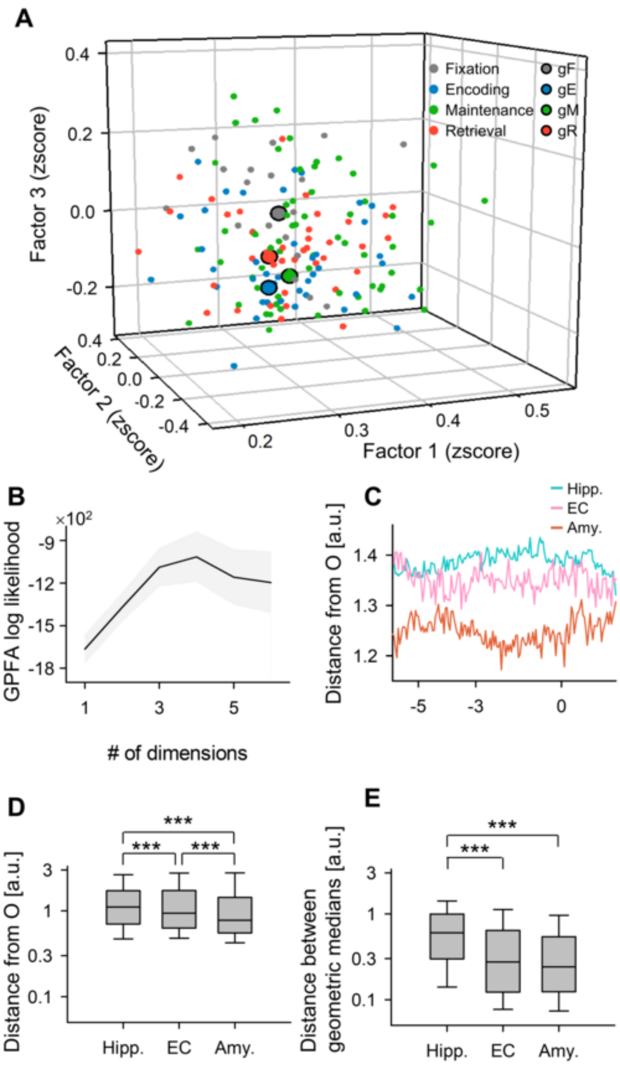


**Figure 2 – State-Dependent Trajectories of Hippocampal Neurons**

***A.*** ~~Neural~~ This panel depicts neural trajectories within the ~~initial~~ first three-dimensional factors derived from ~~the~~ Gaussian Process Factor Analysis (GPFA)~~are displayed~~. ~~The smaller~~ Smaller dots ~~correspond to~~ represent coordinates ~~of~~ corresponding to 50-ms neural trajectory bins. Meanwhile, ~~while the~~ larger dots with *black* ~~edges signify the~~ borders denote geometric medians for ~~respective~~ different stages in the Sternberg working memory task, as follows: fixation (*gray*), encoding (*blue*), maintenance (*green*), and retrieval (*red*). ***B.*** The ~~figure conveys~~ graph presents the log-likelihood of the GPFA models ~~versus~~ compared with the ~~count~~ number of dimensions used to embed multiunit spikes ~~found in~~ from the medial temporal lobe (MTL) territories. ~~In specific~~Specifically, the ~~elbow method pinpointed the~~ optimal dimension, as indicated by the elbow method, was found to be three. ***C.*** This ~~panel~~ figure illustrates the distance of the neural trajectories from the origin (*O*) for the hippocampus (Hipp.), entorhinal cortex (EC), and amygdala (Amy.), ~~against the~~ over time ~~elapsed from~~ following the probe onset. ***D.*** The ~~distance~~ panel displays distances of the ~~trajectory~~ trajectories from *O* within the MTL ~~regions is displayed~~areas. The hippocampus ~~shows~~ demonstrates the ~~farthest~~ greatest distance, followed by the EC and the Amygdala. ***E.*** ~~The plot represents inter-phase trajectory~~ This graph displays the distances between phases of the trajectories within the MTL regions. Abbreviations:

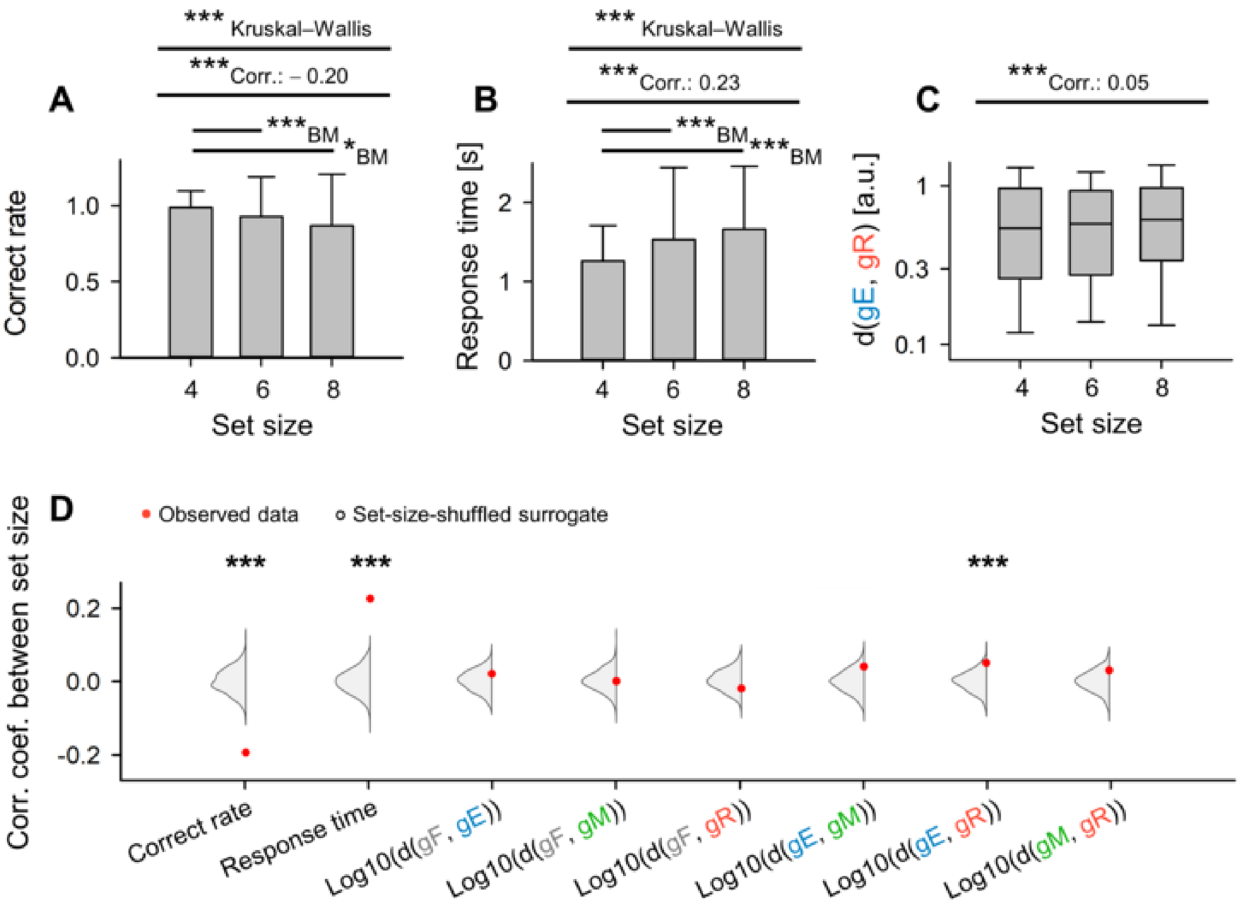


**Figure 3** – ~~**Dependency of Trajectory Distance on Memory Load: Encoding and Retrieval States in Hippocampus**~~ **Dependency of Trajectory Distance on Memory Load: Encoding and Retrieval States in the Hippocampus.**

***A.*** ~~The~~ Illustrates the relationship between set size (the number of letters that ~~need to be encoded~~require encoding) and the correct rate in the working memory task (coefficient = –0.20, ****p* < 0.001). ***B.*** ~~The~~ Showcases the correlation between set size and response time (coefficient = 0.23, ****p* < 0.001). ***C.*** ~~The impact~~ Depicts the influence of set size on the inter-phase distances between the encoding and retrieval phases ($\|g_E g_R\|$) (correlation coefficient = 0.05). ***D.*** *Red* dots represent experimental observations of correlations between set size and the ~~following~~ ensuing parameters: correct rate, response time, $\log_{10}\|g_F g_E\|$, $\log_{10}\|g_F g_M\|$, $\log_{10}\|g_F g_R\|$, $\log_{10}\|g_E g_M\|$, $\log_{10}\|g_E g_R\|$, and $\log_{10}\|g_M g_R\|$. The *gray* kernel density plot ~~illustrates~~ demonstrates the corresponding set-size-shuffled surrogate (*n* = 1,000) (****ps* < 0.001).

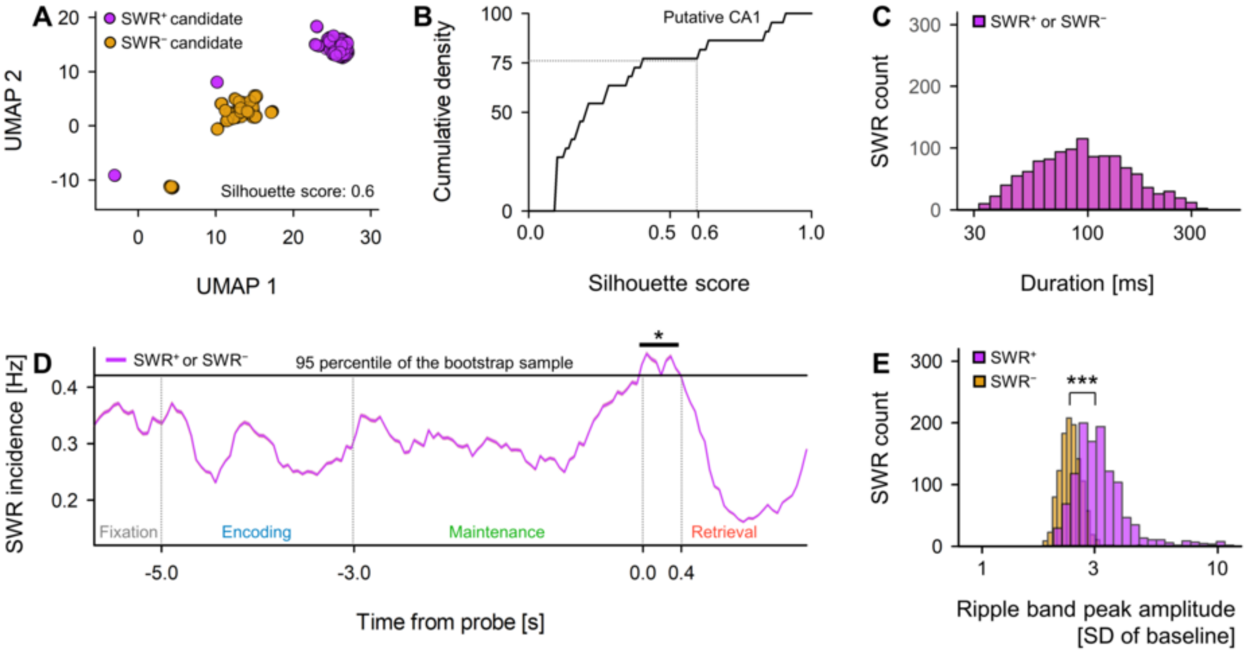


**Figure 4** – ~~**Detection of SWRs in Presumptive CA1 Regions**~~ **Detection of SWRs in Prospective CA1 Regions**

***A.*** ~~Two-dimensional~~ A two-dimensional UMAP (Uniform Manifold Approximation and Projection) [41] projection ~~of~~ that utilizes multiunit spikes is presented during SWR$^+$ candidates (*purple*) and SWR$^-$ candidates (*yellow*). ***B.*** ~~Cumulative~~ A cumulative density plot ~~shows~~ displaying silhouette scores, indicative of the UMAP clustering quality, is provided for hippocampal regions (~~see~~ Table 2 ~~for~~ as reference). ~~Note that hippocampal~~ Hippocampal regions ~~with~~ that exhibit silhouette scores greater than 0.60~~(~~, equivalent to the 75$^{th}$ percentile~~) were~~ , are identified as ~~possible~~ probable CA1 regions. SWR$^+$ and SWR$^-$ candidates ~~recorded~~ obtained from these ~~speculative~~ hypothetical CA1 regions ~~were~~ are respectively ~~classified~~ categorized as SWR$^+$ and SWR$^-$ (with $ns$ = 1,170). ***C.*** The ~~identical~~ same distributions of durations are presented for both SWR$^+$ (*purple*) and SWR$^-$ (*yellow*) ~~, owing~~ due to their ~~definitions~~ similar natures (93.0 [65.4] ms, expressed as median [IQR]). ***D.*** An illustration of the SWR incidence for both the SWR$^+$ (*purple*) and SWR$^-$ (*yellow*) ~~obtained~~ relative to the probe's timing is ~~illustrated~~ conveyed as a mean with a 95% confidence interval. However, ~~as~~ given that the intervals may not be ~~visible~~ noticeable due to their ~~narrow~~ slender range, ~~note~~ it should be highlighted that a significant ~~increase~~ rise in SWR incidence was ~~detected~~ discovered during the ~~initial~~ beginning 400 ms of the retrieval phase (0.421 [Hz], $*p < 0.05$, verified by a bootstrap test). ***E.*** The distributions of ripple band peak amplitudes for SWR$^-$ (*yellow*; 2.37 [0.33] SD of baseline, median [IQR]) and SWR$^+$ (*purple*; 3.05 [0.85] SD of baseline, median [IQR]) are ~~delineated~~ outlined ($***p < 0.001$, confirmed by the Brunner–Munzel test).

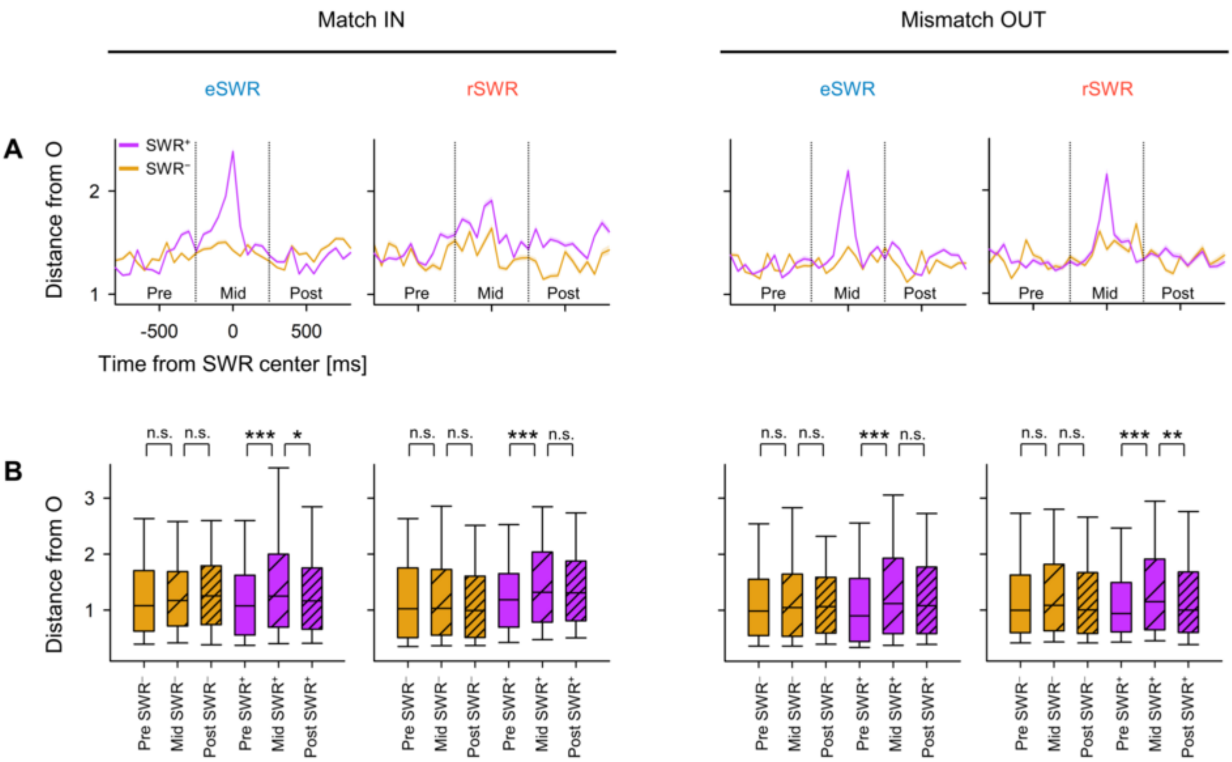


**Figure 5** – ~~**Transient Alterations in Neural Trajectory During SWR Events**~~ **Transient Changes in Neural Trajectory During SWR Events**

***A.*** ~~Displayed~~ Depicted is the distance from the origin ($O$) of the peri-sharp-wave-ripple ~~trajectory~~ (SWR) trajectory, calculated as the mean ±95% confidence interval~~)~~. The intervals ~~may~~ might not be ~~apparent~~ noticeable due to their ~~slender ranges~~narrow magnitudes. ***B.*** ~~Shown~~ Illustrated is the distance from the origin ($O$) during the pre-, mid-, and post-SWR ~~periods~~ phases (*$p < 0.05$, **$p < 0.01$, ***$p < 0.001$; ~~assessed~~ evaluated using the Brunner–Munzel test). Abbreviations: SWR, sharp-wave ripple events; eSWR, SWR ~~during~~ within the encoding phase; rSWR, SWR ~~while in the~~ during retrieval phase; SWR$^+$, positive SWR event; SWR$^-$, control events for SWR$^+$; pre-, mid-, or post-SWR ~~denote~~ refer to the time intervals from −800 to −250 ms, from −250 to +250 ms, or from +250 to +800 ms, all ~~relative~~ in relation to the ~~center~~ central point of the SWR.

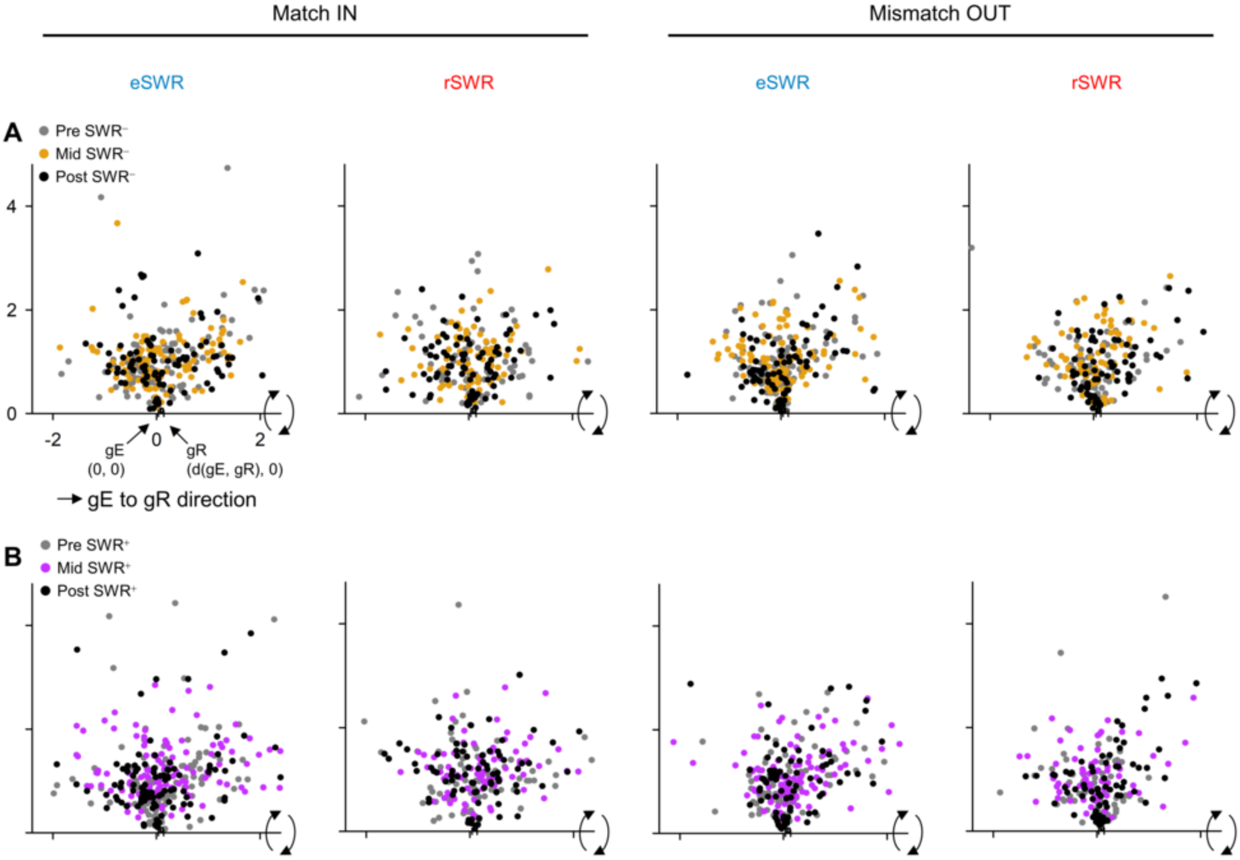


**Figure 6** – ~~**Visualization of Neural Trajectories during SWR in Two-Dimensional Spaces**~~ **Visualizing Neural Trajectories during SWR in Two-Dimensional Spaces**

The ~~panels display~~ figures depict hippocampal neural trajectories during SWR~~as~~, projected onto two-dimensional spaces. ***A.*** ~~Indicates~~ Displays hippocampal neural trajectories ~~pre-SWR$^-$~~ before (~~*gray*~~pre), ~~mid-SWR$^-$~~ during (~~*yellow*~~mid), and ~~post-SWR$^-$~~ after (~~*black*~~post) SWR$^-$, denoted in *gray*, *yellow*, and *black*, respectively. ***B.*** ~~Represents~~ Shows the ~~equivalents~~ corresponding trajectories for SWR$^+$~~as opposed to SWR$^-$~~. The magnitude of $||g_E g_R||$ varied ~~among~~ across sessions. The following projection method was ~~applied in the following manner~~employed: ~~First~~Firstly, a linear transformation positioned $g_E$ at ~~the~~ origin $O$ (0,0), and $g_R$ at ($||g_E g_R||$, 0). The point cloud was then rotated around the $g_E g_R$ axis (~~equivalent~~ identical to the ~~x axis~~x-axis) ~~for fitting~~ to fit into the two-dimensional spaces. ~~Therefore~~Consequently, within these two-dimensional spaces, ~~both~~ the distances from $O$ and the angles ~~preserved~~ remained consistent with the original ~~makeup~~ properties of the $g_E g_R$ axis ~~from~~ in the ~~original~~ three-dimensional spaces. Abbreviations: SWR ~~signifies~~ refers to sharp-wave ripple events; eSWR ~~denotes~~ represents SWR during the encoding phase; rSWR ~~indicates~~ denotes SWR during ~~the~~ retrieval phase; SWR$^+$ ~~,~~ ~~marks~~ indicates an occurrence of SWR event; SWR$^-$ refers to control events for SWR$^+$; pre-SWR, mid-SWR, or post-SWR ~~,~~ ~~reference the~~ refer to time intervals from −800 to −250 ms, from −250 to +250 ms, or from +250 to +800 ms from the center of SWR, respectively.

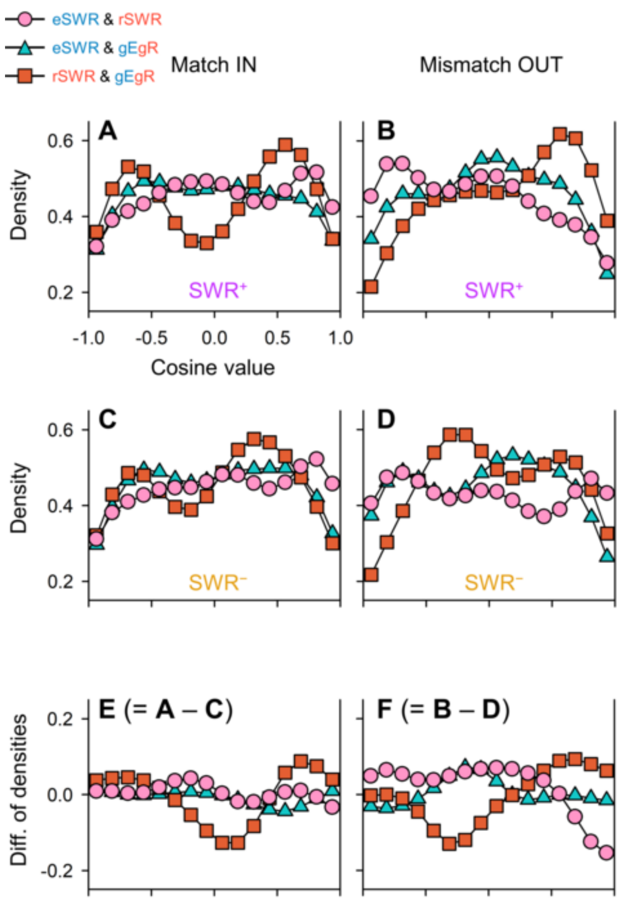


**Figure 7** – ~~**Directions of Neural Trajectories during SWRs Based on Encoding and Retrieval States**~~ **Neural Trajectory Directions during SWRs: Encoding and Retrieval States**

***A–B*** Kernel density estimation (KDE) distributions of $\overrightarrow{\mathrm{eSWR}^{+}} \cdot \overrightarrow{\mathrm{rSWR}^{+}}$ (*pink circles*), $\overrightarrow{\mathrm{eSWR}^{+}} \cdot \overrightarrow{g_{E}g_{R}}$ (*blue triangles*), and $\overrightarrow{\mathrm{rSWR}^{+}} \cdot \overrightarrow{g_{E}g_{R}}$ (*red rectangles*) ~~in~~ are shown for Match ~~In~~ IN (*A*) and Mismatch OUT tasks (*B*). ***C–D*** ~~Present~~ Display the corresponding distributions of SWR⁻ ~~instead of~~ replacing those of SWR⁺ in *A* and *B*. ***E–F*** ~~Depict~~ Illustrate the ~~differences~~ discrepancies in the distributions of SWR⁺ and SWR⁻, ~~illuminating~~ highlighting the SWR components ($E = C - A$; $F = D - B$). ~~Note~~ Observe the biphasic distributions of $\overrightarrow{\mathrm{rSWR}^{-}} \cdot \overrightarrow{g_{E}g_{R}}$, ~~suggesting~~ indicating fluctuations between the encoding and retrieval states ~~during~~ throughout the Sternberg task. ~~Moreover~~Additionally, ~~inverse~~ contrasting directionality between $\overrightarrow{\mathrm{eSWR}^{+}}$ and $\overrightarrow{\mathrm{rSWR}^{+}}$ was ~~observed~~ noticed (*pink circles*) in the Mismatch OUT task, but ~~not~~ was absent in the Match IN task (***E–F***). ~~Finally~~Lastly, ~~shifts~~ transitions from the retrieval to the encoding states were ~~evident~~ prominent in the SWR components in both the Match IN and Mismatch OUT tasks (*red rectangles* in *E* and *F*).